Molecular Vision 2021; 27:608-621 <http://www.molvis.org/molvis/v27/608>
Received 15 October 2020 | Accepted 17 November 2021 | Published 19 November 2021

Mapping retinal ganglion cell somas in a large-eyed glaucoma model

Sara A. Adelman,[1] Kazuya Oikawa,[1,2] Gopika Senthilkumar,[2] Ralph Møller Trane,[2] Leandro B.C. Teixeira,[3] Gillian J. McLellan[1,2]

[1]Department of Surgical Sciences, School of Veterinary Medicine; [2]Department of Ophthalmology & Visual Sciences, School of Medicine and Public Health; [3]Department of Pathobiological Sciences, School of Veterinary Medicine, University of Wisconsin-Madison

Purpose: The purpose of this study was to identify a robust, representative region of interest (ROI) for studies of retinal ganglion cell (RGC) soma loss in feline congenital glaucoma (FCG), a spontaneous, large-eyed glaucoma model.
Methods: Seven FCG and three wild-type (wt) eyes were collected from 10 adult cats of both sexes. Eyes enucleated postmortem were immediately fixed overnight in 4% paraformaldehyde and then stored in 0.1 M PBS at 4 °C. The retinas were wholemounted, Nissl stained with cresyl violet, and imaged using light microscopy. Somas of RGCs were manually identified according to long-established morphological criteria and quantified using a semiautomated method; their coordinates were used to create density maps and plots of the retinal topography. The RGC axon counts for the corresponding eyes were obtained from glutaraldehyde-fixed, resin-embedded optic nerve cross-sections stained with 0.1% p-phenylenediamine (PPD) using a semiautomated counting method. Correlations between total optic nerve axons and RGC soma counts were assessed by linear regression. A k-means cluster algorithm was used to identify a retinal ROI, with further definition using a probability density algorithm.
Results: Interindividual variability in RGC total soma counts was more pronounced in FCG cats (mean = 83,244, range: 0–155,074) than in wt cats (mean = 117,045, range: 97,373–132,972). In general, RGC soma counts were lower in FCG cats than they were in wt cats. RGC axon counts in the optic nerve cross-sections were lower than, but strongly correlated to, the total RGC soma count across all cats (in wt and FCG retinas; $R^2 = 0.88$) and solely FCG eyes ($R^2 = 0.92$). The k-means cluster algorithm indicated a region of the greatest mean difference between the normal wt retinas and FCG-affected retinas within the temporal retina, incorporating the region of the area centralis.
Conclusions: As in other species, RGC soma count and topography are heterogeneous between individual cats, but we identified an ROI in the temporal retina for future studies of RGC soma loss or preservation in a large-eyed model of congenital glaucoma. Many of the methods refined and established to facilitate studies in this FCG model will be broadly applicable to studies in other large-eyed models.

Glaucoma, which is recognized as a leading cause of irreversible blindness worldwide [1], is defined as retinal ganglion cell (RGC) neuropathy and is often associated with abnormally high intraocular pressure (IOP). Animal models used to study glaucoma emulate multiple causes of RGC cell injury associated with glaucoma. Depending on the nature of the experimental model studied, loss of RGC somas may not be highly predictable, with regional and RGC population variation in terms of susceptibility to glaucomatous damage. In the rat microbead ocular hypertension model, for example, the peripheral retina has a relatively higher percentage of RGC soma loss compared with other regions, which is appreciable beginning 6 weeks after microbead injection [2]. The nonhuman primate argon laser ocular hypertension model has a greater RGC soma loss in the ventral retina and greater loss of large RGCs [3]. In a DBA/2J mouse model of glaucoma, regional or diffuse loss of RGC somas may be seen. A distinct pattern occurs in some mice; they develop a wedge of RGC soma loss beginning at 8–10 months that progresses to diffuse, severe soma loss. However, this wedge of RGC soma death is not in a consistent retinal region between individuals [4]. In a study of primary open-angle glaucoma in humans, a paracentral region of RGC soma loss was reported in affected individuals [5]. It has also been suggested that humans with glaucoma have a more susceptible population of RGCs, but the precise nature of the susceptible RGC population remains controversial [6,7].

Since RGC loss is ultimately responsible for irreversible vision loss in glaucoma patients, it is important to have methods of RGC quantification in experimental models of glaucoma. In this study, we examined RGC soma loss in a spontaneously arising model of inherited feline congenital glaucoma (FCG), which has been established in a viable breeding colony. Significant IOP elevation is evident by 10

Correspondence to: Gillian J. McLellan, Department of Ophthalmology and Visual Sciences Medical Sciences Center, 1300 University Avenue, Madison, WI, 53706; Phone: +1 (608) 265-9848; email: gillian.mclellan@wisc.edu

weeks of age in this model, but there is variability in IOP exposure, disease progression, and onset of substantial loss of axons (surrogates also quantified in vivo by optical coherence tomography [OCT] and visual evoked potentials [VEP]), as well as "baseline" RGC/axon counts, in young cats, in common with humans and nonhuman primate models [8-10]. The recessively inherited causal mutation in the *LTBP2* gene identified in FCG-affected cats is an ortholog of a form of primary congenital glaucoma affecting humans (Online Mendelian Inheritance in Man [OMIM] 602091) [11-13]. Given the variable pattern of RGC soma loss documented between individuals and the etiologies of spontaneous and experimental glaucomas in previous studies in other species, the initial assessment of RGC soma loss in the FCG model requires evaluation of the entire retina topography in normal and affected subjects. This analysis is further complicated by the markedly uneven distribution of RGC somas characteristic of the normal feline retina, which is similar to that seen in the central and peripheral retinas in humans [14] and nonhuman primates [15]. In the feline retina, there is a nasal-temporal, horizontal line of increased RGC density called the visual streak and an oval or tear-drop-shaped region in the central temporal retina containing the peak density of RGC somas and photoreceptors, known as the area centralis [16]. Further, the large size of the feline retina diameter (26.5 mm) [17], which is more similar in size to the retina of the rhesus macaque (30 mm) [18] or human (41.5 mm) [18] than the mouse retina (4.5 mm) [19], makes tissue handling, RGC soma quantification, and distribution analysis of the entire retina both technically challenging and time consuming.

In this study, our goal was to identify the region of the retina exhibiting the most consistent RGC soma loss in FCG to enable a more targeted RGC soma quantification, if appropriate. At the time this study was initially conducted, a sensitive and specific immunolabel for feline RGC somas had yet to be validated. Therefore, we used long-established methods for Nissl staining with cresyl violet and manual identification of RGC somas coupled with a rigorous approach that quantified and located all morphologically identified RGCs across the entire retina wholemount. This process proved time intensive, taking a minimum of 50–70 h for the total quantification of RGC somas in each retina. We adapted existing methods to establish more efficient and practical means of quantifying and mapping RGC somas across the relatively large feline retina. Identification of a more specific region of interest (ROI) would limit the need for entire retinal wholemount processing in future studies, allowing remaining neurosensory retina tissue to be available for other investigations, for example, of protein or gene expression.

METHODS

Subjects: Ten retinas were dissected from archived globes of three normal, wild-type (wt) cats and seven FCG-affected cats homozygous for a mutation in the *LTBP2* gene from an established spontaneous FCG colony [8]. Subjects were adult cats of both sexes (Table 1) with disease that appeared to span a range of clinical severity. All animals from which tissues were obtained were maintained in a vivarium in controlled environmental conditions with a 12 h:12 h light-dark cycle under protocols approved by the University of Wisconsin-Madison or Iowa State University Institutional Animal Care and Use Committee (IACUC) and in compliance with the Association for Research in Vision and Ophthalmology (ARVO) Statement on the Use of Animals in Ophthalmic and Vision Research. Globes were enucleated less than 4 h postmortem following euthanasia and fixed in 4% paraformaldehyde at 4 °C overnight; they were then stored in 0.1 M PBS 1X (137 mM NaCl, 2.7 mM KCl, 4.3 mM Na_2HPO_4, 1.47 mM KH_2PO_4; pH 7.4) at 4 °C until further dissection. The wt retinas were collected from cats euthanized for reasons unrelated to the current study.

Retinal wholemount preparation and staining: The technique for dissection of the retina from the globe was conducted according to previously published methods for wholemounting the feline retina [16] with minor modifications. After orienting the globe using the course of the long posterior ciliary arteries, medial origin of the feline nictitating membrane, and course of the attached optic nerve, the eye was hemisected at the ora ciliaris retinae. The vitreous body was removed, and the posterior cup was placed in a glass Petri dish. Under a dissecting microscope (Leica M60, Leica, Wetzlar, Germany), the sclera, choroid, and optic nerve were removed with fine jewelers' forceps and Vannas scissors. The retina was then mounted, with the inner retinal surface uppermost, onto a 50 × 75 mm gelatin-coated glass microscope slide (FD Neurotechnologies, Inc., Columbia, MD), and relief cuts were made to allow the retinal tissue to lie flat (Figure 1A). Remaining attachments of the vitreous at the ora ciliaris retinae and around the optic nerve head location were carefully removed using fine natural hair paintbrushes, Vannas scissors, and small pieces of microfiltration paper. Each slide was placed flat to dry slowly at room temperature overnight in a covered glass staining jar.

Once adhered to the slide, the retina was stained using established methods previously published for Nissl staining of retina wholemounts with 0.25%–0.3% cresyl violet solution (FD Cresyl Violet Solution, PS102–1, FD Neurotechnologies, Inc.) [21]. Briefly, the slide with the affixed retina was submerged in xylenes for defatting and then rehydrated in a

series of solutions with descending concentrations of ethanol. Cresyl violet solution was then gently painted on the surface of the retina with a round-tipped, natural hair paintbrush and allowed to sit for 7–10 min. The stain was rinsed off with deionized water, and the still-wet slide was observed under a light microscope (Leica DM750, Leica) to confirm adequate Nissl staining (Figure 1B); in the event of poor staining, this would permit reapplication of cresyl violet if necessary. The tissue was then dehydrated with ascending concentrations of ethanol solutions. A glacial acetic acid and ethanol solution was used for differentiation, and xylenes were again used for a final clearing step of the remaining background stain. A coverslip was applied using a toluene-based mounting medium (Permount™, Fisher Chemical™, Pittsburgh, PA) and sealed with clear nail polish.

Microscopy, imaging, and RGC soma quantification: A light microscope (Olympus® BX60, Olympus Corporation of the Americas™, Center Valley, PA) with an automated stage (ProScan® III, Prior Scientific, Rockland, MA) and proprietary image analysis software (cellSens Dimension®, Olympus Inc.), was used for automated acquisition and stitching of photomicrographs. Each complete retinal wholemount image, obtained with a 20× objective lens, corresponded to 12–14 gigabytes of data. The image was divided into 16 smaller, more manageable fields to facilitate the subsequent quantification of RGC somas.

The RGC somas were first identified manually by a single observer (SAA) using established morphological criteria of characteristic Nissl substance, a ring of cytoplasm around the nucleus, and a nucleolus in those somas with a diameter greater than 12 µm [17,22,23]. Once identified, a 12 µm diameter, circular mark (0, 255, 0 RGB) was placed over the soma (Figure 1C) using image analysis software (ImageJ, NIH, Bethesda, MD) [24]. When quantification was complete, each image was converted into an 8-bit greyscale image, thresholded to the shade of the markers, converted to a binary image, and scaled to 35% with bicubic interpolation (ImageJ, NIH). The 16 fields were stitched back together to form a single black-and-white image of the entire retinal wholemount (MosaicJ plug-in, ImageJ, NIH) [25]; here, the RGC soma markers were depicted in black and the surrounding retinal tissue in white (Figure 1D.) Each retina was oriented as a left eye for ease of comparison using the characteristic pattern of the feline retinal vasculature (ImageJ, NIH). While the manual quantification was done with care to avoid overlapping RGC soma markers, watershed segmentation performed on the binary image helped to further systematically separate the markers (Watershed tool, ImageJ, NIH). Using the size and circularity of the RGC soma markers, an image analysis tool identified and outlined each marker and tabulated the coordinates of its center (Analyze Particles tool, ImageJ, NIH). After this, regions of the area centralis and central and peripheral retina were assessed to ensure that all RGC somas were counted.

The marker coordinates were binned to create a grid of densities over each retina (Figure 1E; Excel, Microsoft, Redmond, WA). To account for differences in retinal size, the algorithm determined the longest axis of the retina, divided it by 100, and created square bins of that height and width to cover the entire retina with 10,000 bins. Within each bin was the number of RGC soma markers quantified in the bin location of the retina.

Isodensity maps: To facilitate visual assessment of RGC soma distribution/topography, the binned data for the entire retina were input into an open-source software package (R) [26]. For each wholemount, the bin locations were plotted

Table 1. Subject signalment and disease status.

Subject	Sex	Eye	Age (year)	Body weight (kg)
N1	Female	Left	0.8	2.6
N2	Female	Left	1.5	6
N3	Male	Left	2.3	4.9
A1	Female	Right	3.3	3.2
A2	Male	Right	3.8	4.6
A3	Male	Right	4.2	5.8
A4	Male	Right	7.9	4.9
A5	Male	Left	3.3	2.8
A6	Male	Right	2.9	4
A7	Female	Left	3.9	N/A

N=normal wild-type cat, A=Affected cat with feline congenital glaucoma. Bodyweight was not available for subject A7.

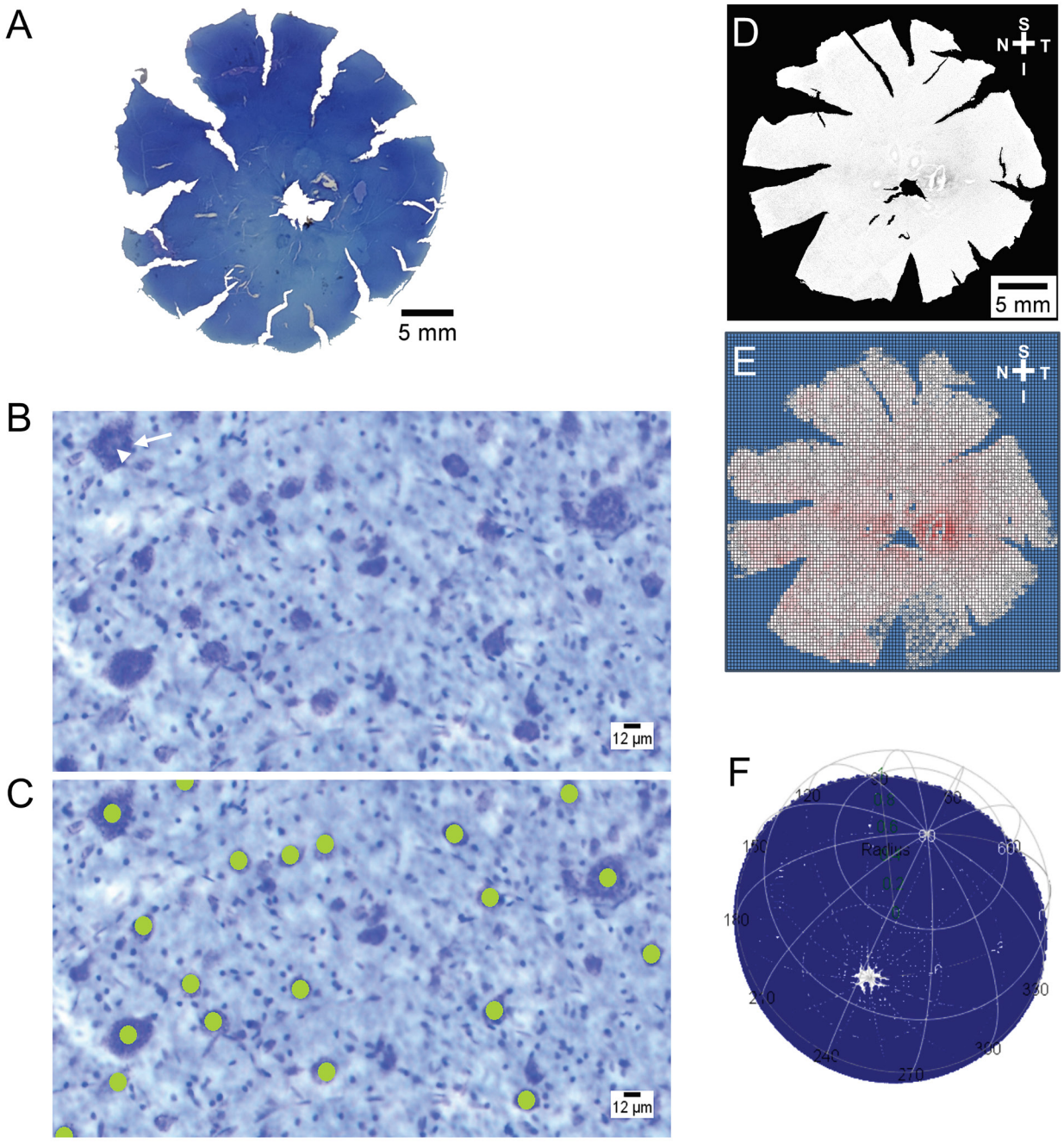

Figure 1. Wholemount preparation and imaging of feline retina. **A:** Image of Nissl-stained retinal wholemount with multiple peripheral retinal relief cuts made to allow the retina to lie flat. **B:** Photomicrograph to illustrate the characteristic Nissl substance (white arrow), ring of cytoplasm, and nucleolus (white arrowhead) of a properly stained retinal ganglion cell (RGC) soma. **C:** Photomicrographs of RGC somas illustrating the manual marking method, with 12 µm circles placed over somas that had the characteristics outlined in (**B**). **D:** Binary image of retinal wholemount (normal wild-type [wt] retina N2) after RGC somas have been identified. "S," "T," "I," and "N" represent the directions of the superior, temporal, inferior, and nasal aspects of the retina, respectively. **E:** Binning of RGC soma counts within 10,000 square bins across the retina (N2; Excel, Microsoft). **F:** Plotting of bin locations on a three-dimensional globe (Retina, R, R Development Core Team).

onto a three-dimensional eyecup (Figure 1F), from which a two-dimensional topographic map with isodensity lines was created (Retistruct and Retina packages, R, R Development Core Team, Auckland, New Zealand).

Quantifying RGC axons: Cross-sections of the corresponding retrobulbar optic nerves were obtained 2–4 mm posterior to each globe, glutaraldehyde postfixed, and routinely osmicated and resin embedded. The myelin sheaths were stained with 1% p-phenylenediamine (PPD) to facilitate the counting of the RGC axons. Quantification was performed using a published, semiautomated targeted sampling method for RGC axon counting that was previously validated for our model using proprietary image analysis software (Olympus cellSens, Dimensions®) [27,28].

Statistical analyses: Descriptive statistics included mean, median, standard error of the mean (SEM), and range for total RGC soma counts, total RGC axon counts, peak RGC soma density (RGC somas/mm^2), and center of area centralis RGC soma density (RGC somas/mm^2). A linear regression model was used to examine the strength of the correlation between total RGC axon and soma counts (GraphPad Prism 7.04, GraphPad Software).

To identify an ROI, the binned density data for three normal wt retinas (N1–3) and five FCG-affected retinas (A3–7) were plotted as density heat maps. Two FCG-affected retinas were excluded from analysis: A1 was excluded because of diffuse, severe RGC soma loss associated with end-stage glaucoma, and A2 was excluded because the location of a relief cut precluded topographic analysis. The RGC soma density maps were then averaged for each bin in the normal (wt) and FCG-affected groups, giving each bin a mean density for the group. A differences map was then calculated by subtracting the mean density of the FCG-affected group from the mean density of the normal wt group for each bin location. To detect a region with higher differences in means between the normal wt and FCG-affected groups, the k-means clustering algorithm was performed using the differences heat map. This algorithm divided each plot into k regions of bins, where the variation between bins within a region was smaller than the variation between regions [29]. This was done in such a way that each bin was assigned to the group in which it was closest to the center. As outlined for difference mapping above, this algorithm was applied to the data from three normal wt retinas (N1–3) and five FCG-affected retinas (A3–7) with k = 2,3,9. All figures and analyses to determine ROI were performed in R (R, R Development Core Team).

RESULTS

Total RGC soma counts: As shown Table 2, Figure 2A the mean total RGC soma count of the wt feline retinas was greater than that of the FCG retinas. However, the two highest soma counts in the study were quantified from the FCG retinas (A4, A5). The box-and-whisker plots suggest a bimodal distribution of total RGC soma counts within the FCG group, with three retinas below 45,000 and four retinas above 100,000, in this relatively small population sample.

Total RGC axon counts: As shown Table 2, Figure 2B, for the soma counts, the mean RGC axon count in wt feline optic nerves was greater than that in the FCG optic nerves. However, the highest optic nerve axon count in this study was identified in an FCG-affected cat (A5). Again, for RGC soma counts, the total optic nerve axon counts of FCG cats appeared to follow a bimodal distribution, with three axon counts less than 45,000 and three over 80,000. The morphology of the optic nerve cross-sections was consistent with the axon and soma counts. Pronounced morphologic evidence of axonal damage, with overall decreased optic nerve cross-sectional area and axonal degeneration, was observed in the severely affected FCG subjects (A1, A4, A6; Figure 3A).

Relationship between RGC soma and axon counts: In this study as shown in Figure 3B,C; Table 2, the RGC optic nerve axon counts were generally lower than the corresponding RGC soma counts. A linear regression model comparing RGC soma counts with their axon counts in three wt (N1–3) and six FCG (A1–6) shows a strong correlation ($R^2 = 0.88$; Figure 3B). When the data from the three wt retinas were removed from the model, the RGC soma and axon counts of the six FCG eyes remained strongly correlated ($R^2 = 0.92$; Figure 3C).

RGC topography: As shown Figure 3A, Table 2 except for FCG retina A1, in which there was a diffuse, generalized, near total absence of RGC somas, the isodensity plots revealed an oval-shaped region of highest RGC soma density in the temporal retina. This region is considered to represent the area centralis, which is analogous to the human/primate macula. In addition, most feline retinas exhibited a nasal-temporal, horizontal streak of greater RGC soma density, which is considered to represent the visual streak. Although mean peak RGC soma density was lower in FCG-affected retinas than it was in wt retinas, the mean values were not significantly different between groups (Figure 4A). For each retina, the bin of the highest RGC soma density was located in the region of the area centralis. A 0.17 mm^2 bin that was manually placed at the center of the area centralis revealed an even higher RGC soma density peak for each retina (Figure 4B). However, these peak values for RGC soma density in

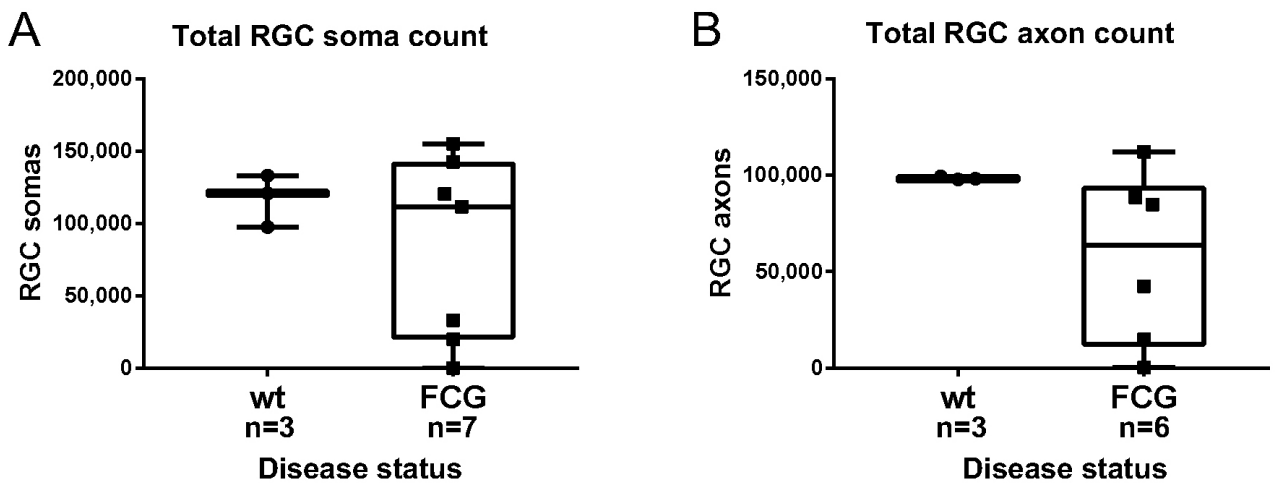

Figure 2. Box-and-whisker plots of mean wild-type (wt) and feline congenital glaucoma (FCG)-affected (**A**) total RGC soma counts (N1–3, A1–7) and (**B**) total RGC axon counts (N1–3, A1–6). The whiskers represent the range of values, and each data point represents the total count for an individual retina/subject. An axon count was not available (N/A) for A7 due to tissue loss during processing.

a more refined region of the area centralis were not statistically significantly different between the wt and FCG-affected groups.

Delineation of ROI: To identify regions of like RGC density difference between the wt and FCG-affected groups, a k-means cluster algorithm was used (Figure 5 and Table 3). For each k (number of regions allowed), the group with the

Table 2. Tabulated data for feline RGC (retinal ganglion cell) soma counts.

Subject	Bin size (mm^2)	Total RGC soma count	Total RGC axon count	Peak density (RGC somas/mm^2)	Center of area centralis (RGC somas/mm^2)
N1	0.108	132972	97653	3009	5453
N2	0.084	120791	99343	1560	3799
N3	0.106	97373	98036	2448	4600
Mean	0.099	117045	98344	2339	4614
Median	0.106	120791	98036	2448	4600
SEM		10446	512	421.83	
A1	0.087	0	297	0	0
A2	0.092	111613	84789	1881	6429
A3	0.063	33135	42438	1968	4224
A4	0.104	155074	88385	2164	5606
A5	0.083	142560	112031	2120	5129
A6	0.041	19989	14964	1550	1347
A7	0.067	120337	N/A	1985	2277
Mean	0.077	83244	57151	1667	3573
Median	0.083	111613	63614	1968	4224
SEM		24054	18239	287.94	

The table shows bin size, total RGC soma count, total RGC axon count, peak RGC soma density, and peak density of RGC somas in area centralis center within a 0.17mm^2 field. Descriptive statistics are presented for 3 normal(N), wt retinas (N1–3) and 7 FCG-affected (feline congenital glaucoma affected; A1–7). An axon count was not available (N/A) for A7 due to tissue loss during processing. (SEM=Standard Error of Mean).

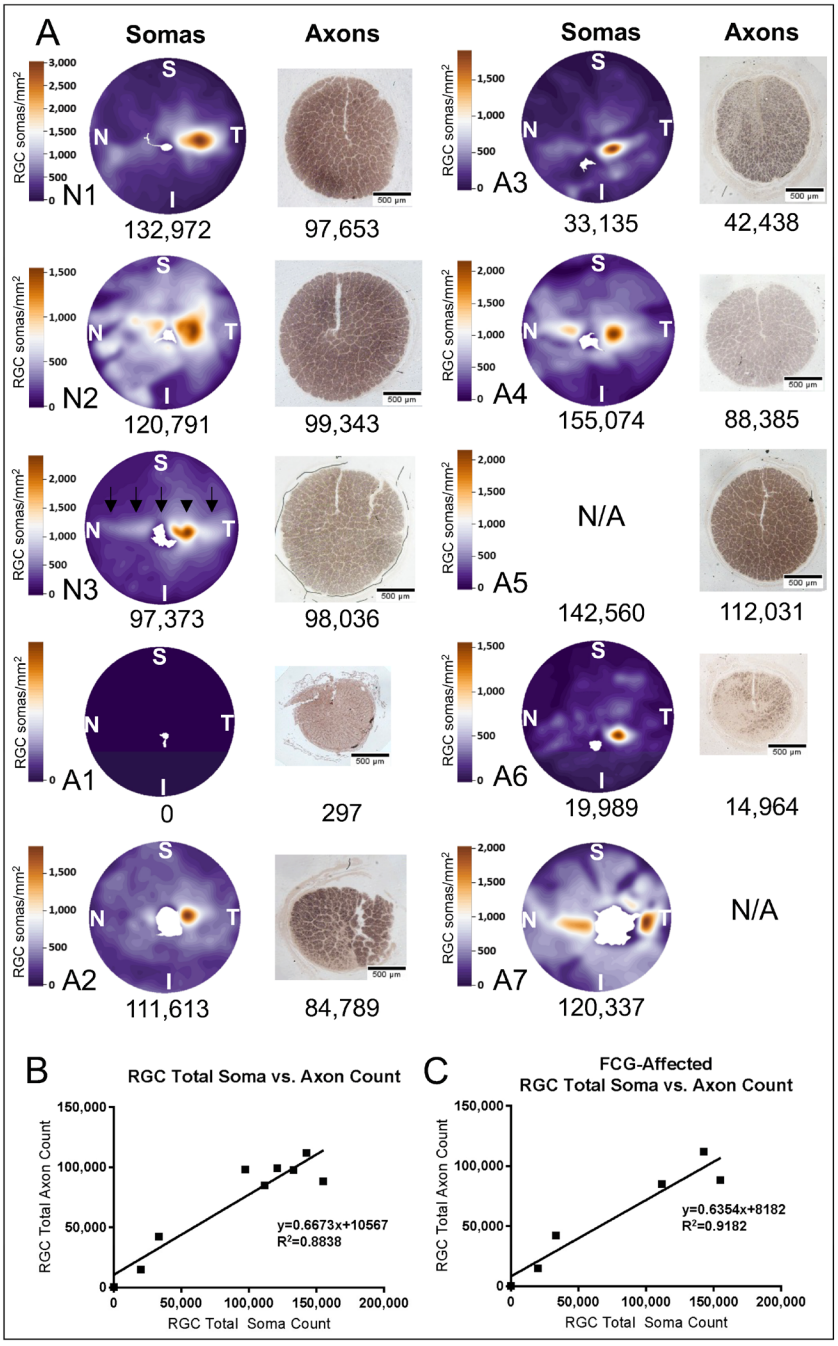

Figure 3. Distribution of RGC densities in normal and glaucomatous feline retinas. **A:** Two-dimensional RGC soma isodensity plots (Retina package, R) for three normal, wild-type (wt) retinas (N1–3) and six feline congenital glaucoma (FCG)-affected retinas (A1–4, A6–7). Regions of higher soma density are represented by warmer colors. Note that the scales assigned to these colors differ between individual retinas. The nasal to temporal visual streak (black arrows, N3) and the area centralis (black arrowhead, N3) are the regions of highest RGC soma density in most normal and FCG-affected retinas. "S," "T," "I," and "N" represent superior, temporal, inferior, and nasal aspects of the retina, respectively. Photomicrographs are also shown of corresponding p-phenylenediamine (PPD)-stained optic nerve cross-sections with their RGC axon counts. [Scale bar = 500 µm; N/A = not available because of tissue damage or loss during processing (A7 ON photomicrograph) or relief cut placement (A5 isodensity plot).] **B:** Linear regression model of total RGC soma versus axon count in three normal wt eyes (N1–3) and six FCG-affected eyes (A1–6). There is a strong correlation ($R^2 = 0.88$) between total RGC soma and axon counts. **C:** Linear regression model of total RGC soma versus axon count in 6 FCG-affected eyes. There is a strong correlation ($R^2 = 0.92$) between total RGC soma and axon counts within the FCG-affected retinas.

highest mean difference was characterized by the coordinates of the center, the mean difference, and the size (Table 3). Total variation within groups and total variation between groups are listed for each k, together with the proportion of the total variation between groups. This latter metric should be as high as possible because this indicates that the groups defined by the algorithm are more different than similar, which is what is desired when refining regions for RGC quantification in disease models.

Picking the appropriate k cluster was challenging because the proportion of the total variation explained by the variation between groups increases when k increases. In this study, one could argue that after k = 7, the proportion of the total variation stabilized just above 81%. However, the region identified by this algorithm as the region with the largest difference was rather consistent. For k > 4, most of the region is located over the area centralis (Figure 5C). Hence, the specific k is less important because we were mainly interested in identifying a useful region for future studies.

Probability density analysis: Figure 6: A region of the retina that consistently included the k cluster with the largest RGC density difference was defined using a Cartesian coordinate system with x and y axes and the center of the retina at (0,0). To facilitate this process, all images of whole retinas were oriented as left eyes and rotated using characteristic vasculature, as noted previously. The first ROI (ROI 1) was then delineated starting along the positive y-axis and extending 135° clockwise for the inferior boundary to land in the temporal-inferior retina (Figure 6A). The probability density plot (Figure 6B) of this wedge did not demonstrate a large difference in density distribution between the normal and FCG-affected retinas. The second ROI (ROI 2) decreased the size of ROI 1 by including only those bins located within a 25 bin radius from the center of the retina (0,0), creating an arc and removing the peripheral retina from the analysis (Figure 6C). On the probability density plot for ROI 2 (Figure 6D), a far more discernable separation in the density distribution between the wt and FCG-affected groups could be appreciated, with a shift toward higher densities in the normal wt retinas.

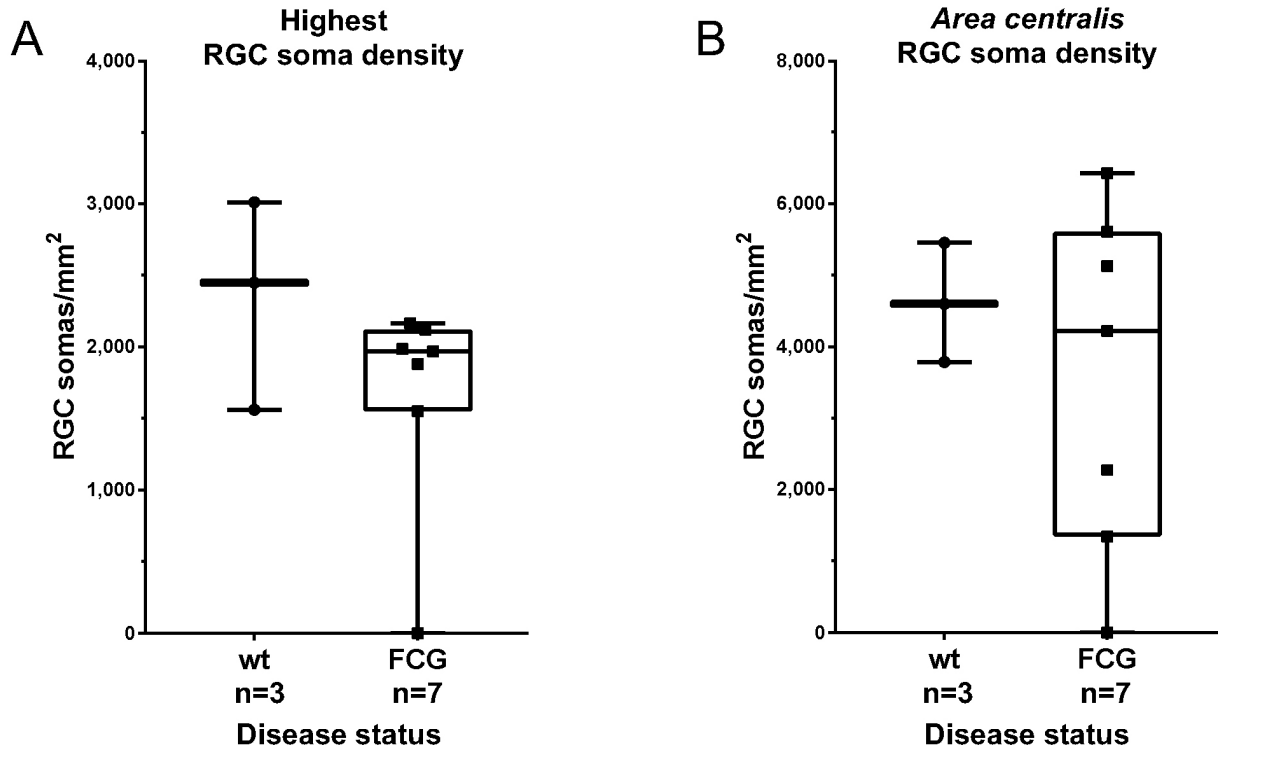

Figure 4. Peak RGC densities. Box-and-whisker plots of the highest RGC soma densities in (**A**) the area centralis and (**B**) a more defined 0.17 mm^2 bin in the center of the area centralis. The smaller bin (0.17 mm^2) was manually placed in the center of the area centralis, defined using vasculature and the highest apparent density. The whiskers represent the range of values, and each data point shown represents the cell density calculated for an individual eye/subject. There was no statistically significant difference in mean densities between the normal wild-type (wt), and feline congenital glaucoma (FCG)-affected groups for either metric.

DISCUSSION

The total counts of RGC somas for the wt retinas in this study were within an expected range based on previously published data for normal cats. The total RGC soma counts in normal cats have been reported to range widely, spanning from 90,000 to 260,000, with a larger variation seen between than within studies [17,23,30-32]. Discrepancies between studies are likely primarily due to methodological differences; however, there is interindividual variation expected, which was evident in this study. Few, if any, published studies on RGC soma density and distribution in the normal feline retina present a total direct count of RGC somas; rather, they

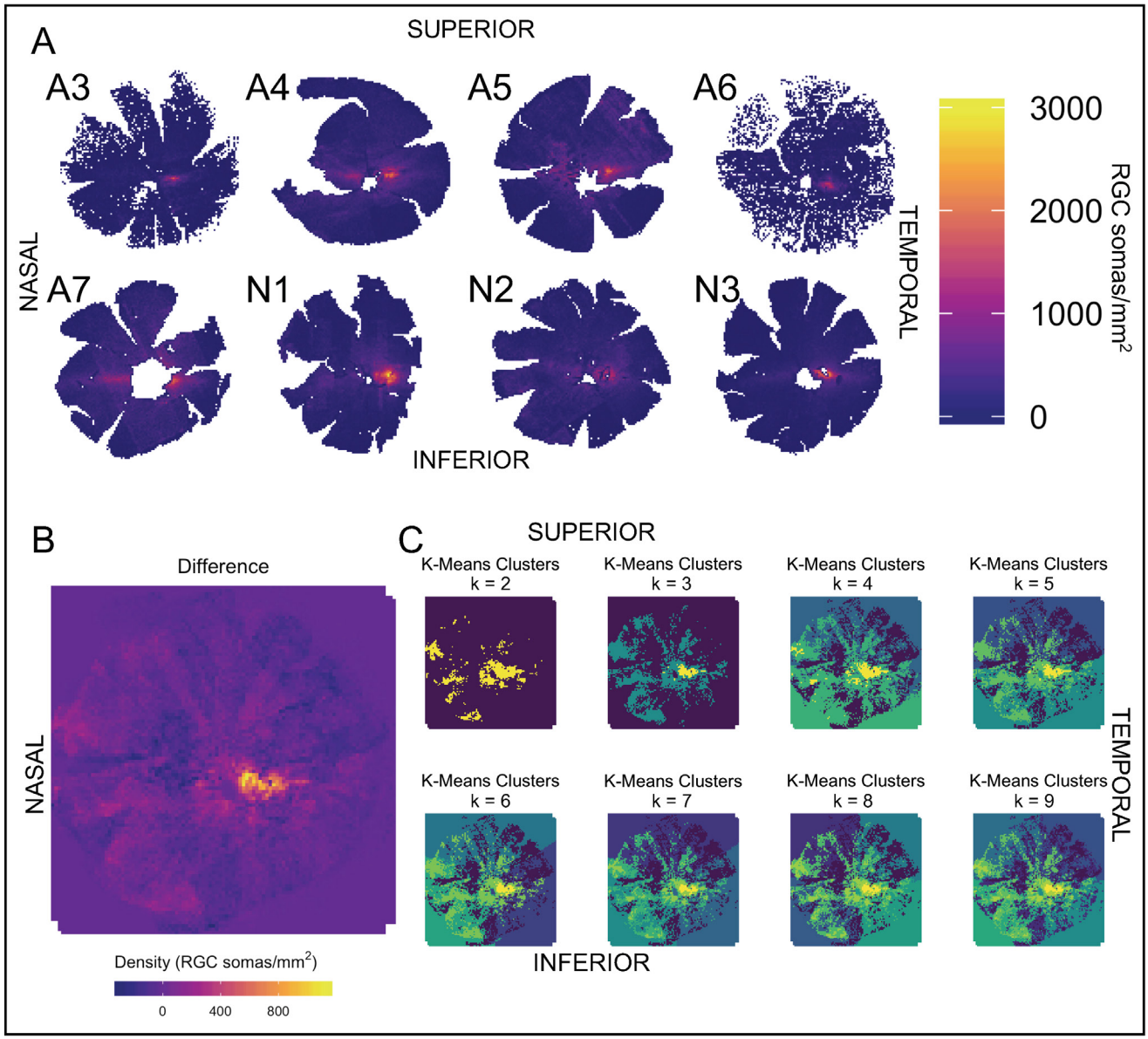

Figure 5. Heat maps of RGC densities. **A:** Density topography of RGC somas in three normal wild-type (wt) retinas (N1–3) and five feline congenital glaucoma (FCG)-affected retinas (A2–6). In all retinas, the area of highest density, or the warmest colors, can be seen in the region of the area centralis, temporal to the location of the optic nerve head. **B:** Density heat map of the difference between the regional mean of the normal wt group and the FCG-affected group (i.e., normal minus affected). The groups did not seem to differ substantially within the peripheral retina. The largest difference in mean RGC soma densities between groups (warmest colors) can be seen in the region of the area centralis. **C:** K-means cluster algorithm with clusters 2–9. Throughout all the groups, the k-means cluster algorithm indicates the area of least regional variability in between-group differences in soma density within the temporal retina, associated with the area centralis.

often estimate the number of somas in the retina based on sampling fields. With such a dramatically uneven RGC soma distribution across the normal feline retina, using an estimation algorithm based on a lattice of sampling fields has the potential to vastly over- or underestimate the total RGC soma count in each study. The inherent subjectivity of identifying Nissl-stained RGC somas based on morphological criteria may also contribute to discrepancies in counts between studies. In this study, a second observer (GJM) identified a field of RGC somas compared with the same field marked by the primary observer (SAA), validating the primary observer's identification of somas. In addition, to avoid mistaking displaced amacrine cells for RGC somas, in this study, we took a conservative approach and defined RGCs as having a soma diameter greater than 12 µm. A similar approach was applied in previously published papers but without reporting total RGC soma counts [22,33,34]. Displaced amacrine cells, which also contain Nissl substance, comprise 80% of the neuronal cell population in the RGC layer of the feline retina, and have soma diameters from 6 to 10 µm [32], so they would not have been counted by our method. However, we likely failed to count proportionately small populations of RGCs with overlapping somas of smaller diameter [31].

To avoid limitations inherent in our approach for the identification of RGCs, there are other methods of RGC soma labeling that have been used in previously published studies of the mammalian retina that are not as reliant on morphological criteria for identification. Retrograde labeling applies a dye (e.g., horseradish peroxidase [HRP], 1,1'-dioctadecyl-3,3,3',3'- tetramethylindocarbocyanine perchlorate [DiI], fast blue, fluorogold) to a region of the central visual pathway (superior colliculus, lateral geniculate nucleus) to be transported along the RGC axons and into the somas [35]. In the FCG model, in at least some affected animals, there is evidence of significant RGC axonal damage and dysfunction at the onset of disease [36]. Therefore, RGC somas persisting in the retina may not be reliably labeled with this method. In addition, the surgical procedure in a feline model to expose and inject dye into the superior colliculus and lateral geniculate nucleus is invasive, and at the same time, it can result in incomplete labeling [35]. Cholera toxin subunit B (CTB) conjugated to, for example, HRP can label RGC somas by more predictable and less invasive intravitreal injection and anterograde transport mechanisms, but this method has not been extensively validated in feline models, and it still involves a relatively invasive method for in vivo administration [37].

For this study, to quantify and map the entire heterogeneous RGC soma population, an immunolabel with a conjugated fluorescent antibody would be ideal; this would make manual morphological identification of somas unnecessary and thus decrease subjectivity. When this study was performed, a specific antibody was not validated for feline RGCs. The RNA binding protein with multiple splicing (RBPMS) antibody has been validated in other species [38-40] as RGC soma specific. However, the RBPMS antibody initially evaluated for this study did not robustly label RGC somas in a normal feline retina. An RBPMS antibody

Table 3 K. -means cluster analysis metrics for 3 normal, wt retinas (N1–3) and 5 FCG-affected retinas (A3–7).

k	Mean difference in group (RGC somas/mm²)	Size (bins)	Total variation within groups [(RGC somas/mm²)²]e+07	Total variation between groups [(RGC somas/mm²)²] e+07	Proportion of variation between groups
2	217	744	6.78	3.84	0.36
3	577.65	101	4.73	5.9	0.56
4	370.22	257	4.1	6.52	0.61
5	567.92	105	2.81	7.81	0.74
6	616.13	87	2.44	8.18	0.77
7	712.43	60	1.99	8.64	0.81
8	676.66	69	1.77	8.85	0.83
9	725.36	57	1.54	9.08	0.85

This algorithm divides the RGC soma density differences map (Figure 5) into k groups such that bins within the same group are more alike than between the groups. We measured similarity in three dimensions: two locations (row and column) and RGC soma density difference between the wt and FCG-affected groups. In this table, for each k, the group with the highest mean difference is characterized (by coordinates of the center, the mean difference, and the size). Furthermore, the total variation within groups and total variation between groups are listed for each k, together with the proportion of the total variation that is between groups. This latter metric should be as high as possible when looking for the region that varies the most between wt and FCG-affected RGC soma density, as this indicates that the groups defined by the algorithm are more different than similar, which is what is desired.

has since been validated in cats by another group [41] and is now used in our FCG model, but it was not available when this study was conducted.

Total RGC axon counts acquired from light photomicrographs of optic nerve cross-sections for wt animals (range: 97,653 to 98,036 axons) are lower than previously reported feline optic nerve axon counts acquired using electron microscopy (range: 158,000 to 184,000 RGC axons) [42,43]. Our methods, which rely on identification of axons by their myelin sheath staining, inherently undercount axons of smaller diameter. Both of these techniques for axon quantification use algorithms for estimating the total population instead of a direct count. Thus, the techniques used in our study to quantify RGC axons and somas were both expected to systematically underestimate the number of small RGC somas and axons.

In both the total RGC soma and axon counts in this study, the highest values were quantified from the FCG-affected retinas (A4, A5). With the interindividual variability and the range observed in the wt RGC counts, as well as the deliberate selection of FCG cats reflecting a broad range of clinical disease severity, these particular FCG cats may have inherently possessed more RGCs than the three wt cats in this study, and quantification may have occurred before RGC soma losses. Furthermore, it is interesting to note that the distribution of RGC counts (soma and axon) in FCG cats appeared bimodal in nature, with three retinas exhibiting severe RGC loss and three within or above the range determined for wt cats. With such a small sample size, it is difficult to draw conclusions from either of these observations; however, the study does present a population of adult FCG cats that are known to have been clinically affected by

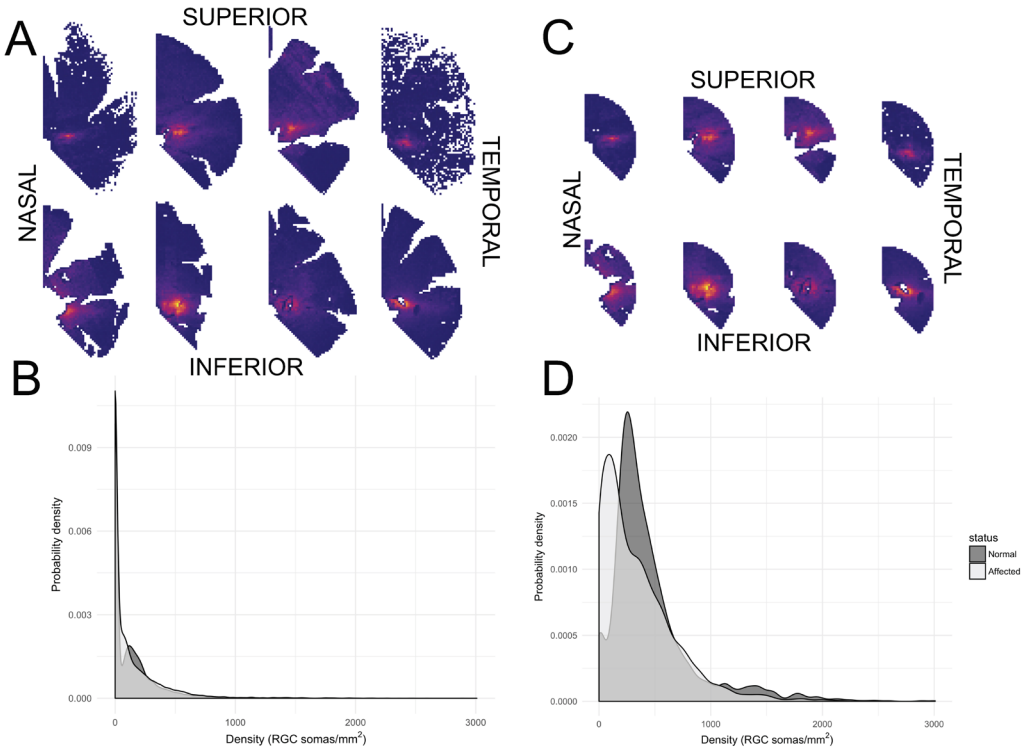

Figure 6. Refining a region of interest (ROI) with greatest difference in RGC density in glaucoma-affected retina. **A**: Region of interest 1 (ROI 1): This region of the heat map was defined by placing the heat map on the Cartesian coordinate system, with the center of the retina at (0,0) and extending 135° clockwise from the positive y-axis. **B:** ROI 1 probability density plot: This plot does not show a large difference in the density distribution between normal wild-type (wt; N1–3; dark gray) and feline congenital glaucoma (FCG)-affected (A3–7; light gray) retinas in this ROI. **C:** Region of interest 2 (ROI 2): This region of the density heat map decreased the size of ROI 1 by measuring 20 bins temporally from the center of the retina and mapping an intersecting vector. **D**: ROI 2 probability density plot: A far more discernable difference in densities between the normal wt (dark gray) and FCG-affected (light gray) groups can be seen on this plot, with a shift toward higher densities in the normal wt retinas. This is likely because most of the artifacts in the peripheral retina inserting bins with 0 somas has been taken away. Differences in the regional mean densities between the groups are negligible in the peripheral retina.

ocular hypertension and that appear to have minimal, if any, RGC loss.

The pattern of uneven distribution of RGC somas found in this study has been documented as characteristic of the feline retina in previously published topographic studies [16]. The RGC soma density peaks in the area centralis presented in this paper are lower than previously published densities ranging between 5,000, and 10,000 RGC somas/mm^2 [23,30,34]. The lower densities in that range, ~5,000 to 6,000 RGC somas/mm^2, are from a study that used the same RGC soma identification criteria, including soma size, as used in this study, but that study quantified the area centralis density by placing a 0.17 mm^2 bin over the center of the area centralis [34]. When applying this smaller bin size and precise location to the retinas sampled in the present study, the area centralis RGC soma density was consistent with that reported previously [34]. This observation supports the underestimation of peak RGC densities in our current study, whether by undercounting a significant population of RGCs with a soma size < 12 µm within the area centralis or use of too large a bin size with imprecise positioning over the area centralis. However, accurate quantification of absolute RGC peak density was less important to the goals of the current study than development of an automated, unbiased binning system to compare regions of the retinas across multiple retinas in a time-efficient manner.

Through RGC mapping and advanced statistical analyses, we identified and refined an ROI to facilitate future studies of RGCs in this model, which limits the need for preparation of flatmounts of the whole retina. Previous studies in a feline optic nerve crush model chose a 1.66 mm^2 region located 3 mm superior and 1.5 mm temporal to the area centralis for evaluation of RGC soma loss in the retina [22,34]. However, that region did not robustly reflect RGC soma loss in the FCG model in this study. Each model is expected to have varying patterns of RGC soma loss due to varying susceptibility of RGC populations to different types of injury, often by mechanisms that remain poorly understood [44,45].

RGCs have been categorized by soma size and morphology, dendritic tree branching [44,45], the on/off center dichotomy [46], and axonal projections. With Nissl stain, the most thoroughly defined populations in α, β, and γ RGCs comprise 3.5%, 47.2%, and 49.2% of the total RGC population, respectively, in a normal feline retina [32], albeit with individual regional density variation [31]. Alpha RGCs make up only 1.6% of the RGC soma population within the area centralis, increasing up to 6.9% of the population in the peripheral retina [23]. Although distinguishing β and γ RGC populations can be challenging due to some overlap of soma diameter, a greater percentage of β RGCs has been reported in the area centralis, and a greater proportion of γ-RGCs has been found in the periphery [31]. Overall, it has been established that not only does a normal cat retina have an uneven distribution of all RGCs, but there is also an uneven distribution within each class of RGCs. The differences in susceptibility to FCG damage between eyes, subjects, retina regions, and RGC types, as well as the influence of age, sex, and IOP on RGC loss in glaucoma, are subject to ongoing, expanded studies in this model, facilitated by identification of a manageable, consistent ROI.

Conclusion: RGC soma counts and distributions are heterogeneous between individual cats, whether they are FCG-affected or normal wt animals. Using our isodensity plots and k-means clustering statistical analysis, an ROI has been identified for future studies of RGC soma loss (or relative preservation) in this FCG model. Future studies using the RBPMS immunolabel—and thus automated quantification—are indicated for further definition of this ROI with a larger sample size. This project established a set of tools to map and analyze the large and unwieldy datasets resulting from quantification of RGC somas in a large-eyed species. While this study was performed in a feline model of glaucoma, these techniques could be applied to other models and species with similarly sized eyes, such as those of common nonhuman primate species and even humans. With the validation of RGC-specific markers, such as RBPMS, in an increasing number of species, quantification of total RGC somas could be further automated, vastly increasing the feasibility of studying RGC soma integrity and distribution in large-eye models. While the wholemounting and quantification techniques performed in this study allow for a morphologic and topographic assessment of RGC somas, RGC axon counts remain a practical means to assess overall RGC damage as it pertains to vision loss in the FCG model of glaucomatous optic neuropathy.

ACKNOWLEDGMENTS

This work was supported in part by NIH T35 OD011078 and a stipend from the School of Veterinary Medicine, UW-Madison (SAA); NIH grants: K08EY018609; UL1TR000427; R01EY027396 (GJM) and Core Grant for Vision Science, P30EY016665, and by an unrestricted award to the UW-Madison Department of Ophthalmology and Visual Sciences from Research to Prevent Blindness. The authors wish to thank Dr. N. Matthew Ellinwood for contribution of tissues from animals in an FCG breeding colony previously maintained at Iowa State University, and Ben August for preparation of semi-thin optic nerve sections. We are

indebted to the following individuals and groups for knowledgeable advice and technical support: Brian Cohn; members of the Comparative Ocular Pathology Lab of Wisconsin; Dr. Joan S. Jorgensen, and Dr. Robert W. Nickells.

REFERENCES

1. Tham YC, Li X, Wong TY, Quigley HA, Aung T, Cheng CY. Global prevalence of glaucoma and projections of glaucoma burden through 2040: a systematic review and meta-analysis. Ophthalmology 2014; 121:2081-90. [PMID: 24974815].
2. Laquis S, Chaudhary P, Sharma SC. The patterns of retinal ganglion cell death in hypertensive eyes. Brain Res 1998; 784:100-4. [PMID: 9518569].
3. Glovinsky Y, Quigley HA, Dunkelberger GR. Retinal ganglion cell loss is size dependent in experimental glaucoma. Invest Ophthalmol Vis Sci 1991; 32:484-91. [PMID: 2001923].
4. Schlamp CL, Li Y, Dietz JA, Janssen KT, Nickells RW. Progressive ganglion cell loss and optic nerve degeneration in DBA/2J mice is variable and asymmetric. BMC Neurosci 2006; 7:66-[PMID: 17018142].
5. Lei Y, Garrahan N, Hermann B, Fautsch MP, Johnson DH, Hernandez MR, Boulton M, Morgan JE. Topography of neuron loss in the retinal ganglion cell layer in human glaucoma. Br J Ophthalmol 2009; 93:1676-9. [PMID: 19671529].
6. Quigley HA, Dunkelberger GR, Green WR. Retinal ganglion-cell atrophy correlated with automated perimetry in human eyes with glaucoma. Am J Ophthalmol 1989; 107:453-64. [PMID: 2712129].
7. Morgan JE. Selective Cell-Death in Glaucoma - Does It Really Occur. Br J Ophthalmol 1994; 78:875-9. [PMID: 7848987].
8. Kuehn MH, Lipsett KA, Menotti-Raymond M, Whitmore SS, Scheetz TE, David VA, O'Brien SJ, Zhao Z, Jens JK, Snella EM, Ellinwood NM, McLellan GJ. A Mutation in *LTBP2* Causes Congenital Glaucoma in Domestic Cats *(Felis catus).* PLoS One 2016; 11:e0154412-[PMID: 27149523].
9. Rutz-Mendicino MM, Snella EM, Jens JK, Gandolfi B, Carlson SA, Kuehn MH, McLellan GJ, Ellinwood NM. Removal of potentially confounding phenotypes from a Siamese-derived feline glaucoma breeding colony. Comp Med 2011; 61:251-7. [PMID: 21819695].
10. Adelman S, Shinsako D, Kiland JA, Yaccarino V, Ellinwood NM, Ben-Shlomo G, McLellan GJ. The post-natal development of intraocular pressure in normal domestic cats (*Felis catus*) and in feline congenital glaucoma. Exp Eye Res 2018; 166:70-3. [PMID: 29054387].
11. Ali M, McKibbin M, Booth A, Parry DA, Jain P, Riazuddin SA, Hejtmancik JF, Khan SN, Firasat S, Shires M, Gilmour DF, Towns K, Murphy AL, Azmanov D, Tournev I, Cherninkova S, Jafri H, Raashid Y, Toomes C, Craig J, Mackey DA, Kalaydjieva L, Riazuddin S, Inglehearn CF. Null mutations in *LTBP2* cause primary congenital glaucoma. Am J Hum Genet 2009; 84:664-71. [PMID: 19361779].
12. Lim SH, Tran-Viet KN, Yanovitch TL, Freedman SF, Klemm T, Call W, Powell C, Ravichandran A, Metlapally R, Nading EB, Rozen S, Young TL. *CYP1B1, MYOC*, and *LTBP2* mutations in primary congenital glaucoma patients in the United States. Am J Ophthalmol 2013; 155:508-17. [PMID: 23218701].
13. Désir J, Sznajer Y, Depasse F, Roulez F, Schrooyen M, Meire F, Abramowicz M. *LTBP2* null mutations in an autosomal recessive ocular syndrome with megalocornea, spherophakia, and secondary glaucoma. Eur J Hum Genet 2010; 18:761-7. [PMID: 20179738].
14. Curcio CA, Allen KA. Topography of ganglion cells in human retina. J Comp Neurol 1990; 300:5-25. [PMID: 2229487].
15. Stone J, Johnston E. The topography of primate retina: a study of the human, bushbaby, and new- and old-world monkeys. J Comp Neurol 1981; 196:205-23. [PMID: 7217355].
16. Stone J. *The Wholemount Handbook*. 1981Maitland Publications, Australia. pp. 127.
17. Stone J. A quantitative analysis of the distribution of ganglion cells in the cat's retina. J Comp Neurol 1965; 124:337-52. [PMID: 4955540].
18. Stone J, Johnston E. The Topography of Primate Retina - A Study of The Human, Bushbaby, and New-World and Old-World Monkeys. J Comp Neurol 1981; 196:205-23. [PMID: 7217355].
19. Drager UC, Olsen JF. Ganglion cell distribution in the retina of the mouse. Invest Ophthalmol Vis Sci 1981; 20:285-93. [PMID: 6162818].
20. Ullmann JF, Moore BA, Temple SE, Fernández-Juricic E, Collin SP. The retinal wholemount technique: a window to understanding the brain and behaviour. Brain Behav Evol 2012; 79:26-44. [PMID: 22142853].
21. Weber AJ, Viswanáthan S, Ramanathan C, Harman CD. Combined application of BDNF to the eye and brain enhances ganglion cell survival and function in the cat after optic nerve injury. Invest Ophthalmol Vis Sci 2010; 51:327-34. [PMID: 19710411].
22. Stone J. The number and distribution of ganglion cells in the cat's retina. J Comp Neurol 1978; 180:753-71. [PMID: 681546].
23. Schneider CA, Rasband WS, Eliceiri KW. NIH Image to ImageJ: 25 years of image analysis. Nat Methods 2012; 9:671-5. [PMID: 22930834].
24. Thévenaz P, Unser M. User-friendly semiautomated assembly of accurate image mosaics in microscopy. Microsc Res Tech 2007; 70:135-46. [PMID: 17133410].
25. Cohn BA, Collin SP, Wainwright PC, Schmitz L. Retinal topography maps in R: new tools for the analysis and visualization of spatial retinal data. J Vis 2015; 15:19-[PMID: 26230981].
26. Teixeira LB, Buhr KA, Bowie O, Duke FD, Nork TM, Dubielzig RR, McLellan GJ. Quantifying optic nerve axons in a cat glaucoma model by a semi-automated targeted

counting method. Mol Vis 2014; 20:376-85. [PMID: 24715755].

27. Marina N, Bull ND, Martin KR. A semiautomated targeted sampling method to assess optic nerve axonal loss in a rat model of glaucoma. Nat Protoc 2010; 5:1642-51. [PMID: 20885376].

28. Kanungo T, Mount DM, Netanyahu NS, Piatko CD, Silverman R, Wu AY. An efficient k-means clustering algorithm: analysis and implementation IEEE Trans Pattern Anal Mach Intell 2002; 24:881-92. .

29. Hughes A. Quantitative-analysis of cat retinal ganglion-cell topography. J Comp Neurol 1975; 163:107-28. [PMID: 1159109].

30. Hughes A. population magnitudes and distribution of the major modal classes of cat retinal ganglion cells as estimated from HRP filling and a systematic survey of the soma diameter spectra for classical neurons. J Comp Neurol 1981; 197:303-39. [PMID: 7276237].

31. Wong ROL, Hughes A. The morphology, number, and distribution of a large population of confirmed displaced amacrine cells in the adult cat retina. J Comp Neurol 1987; 255:159-77. [PMID: 3819013].

32. Weber AJ, Kalil RE. The percentage of interneurons in the dorsal lateral geniculate nucleus of the cat and observations on several variables that affect the sensitivity of horseradish peroxidase as a retrograde marker. J Comp Neurol 1983; 220:336-46. [PMID: 6643731].

33. Weber AJ, Harman CD. BDNF treatment and extended recovery from optic nerve trauma in the cat. Invest Ophthalmol Vis Sci 2013; 54:6594-604. [PMID: 23989190].

34. Kelly JP, Gilbert CD. The projections of different morphological types of ganglion cells in the cat retina. J Comp Neurol 1975; 163:65-80. [PMID: 1159111].

35. Oikawa K, Ver Hoeve JN, Teixeira LBC, Snyder KC, Kiland JA, Ellinwood NM, McLellan GJ. Sub-region-Specific Optic Nerve Head Glial Activation in Glaucoma. Mol Neurobiol 2020; 57:2620-38. [PMID: 32266645].

36. Trojanowski JQ, Gonatas JO, Gonatas NK. Conjugates of horseradish peroxidase (HRP) with cholera toxin and wheat germ agglutinin are superior to free HRP as orthogradely transported markers. Brain Res 1981; 223:381-5. [PMID: 6169406].

37. Kwong JMK, Caprioli J, Piri N. *RNA* Binding Protein with Multiple Splicing: A new marker for Retinal Ganglion Cells. Invest Ophthalmol Vis Sci 2010; 51:1052-8. [PMID: 19737887].

38. Kwong JM, Quan A, Kyung H, Piri N, Caprioli J. Quantitative analysis of Retinal Ganglion Cell survival with Rbpms immunolabeling in animal models of optic neuropathies. Invest Ophthalmol Vis Sci 2011; 52:9694-702. [PMID: 22110060].

39. Rodriguez AR, de Sevilla Müller LP, Brecha NC. The RNA binding protein RBPMS is a selective marker of ganglion cells in the mammalian retina. J Comp Neurol 2014; 522:1411-43. [PMID: 24318667].

40. Wang Y, Wang W, Liu J, Huang X, Liu R, Xia H, Brecha NC, Pu M, Gao J. Protective effect of ALA in crushed optic nerve cat retinal ganglion cells using a new marker RBPMS. PLoS One 2016; 11:e0160309-[PMID: 27504635].

41. Hughes A, Wassle H. The cat optic nerve: fibre total count and diameter spectrum. J Comp Neurol 1976; 169:171-84. [PMID: 965509].

42. Williams RW, Chalupa LM. An analysis of axon caliber within the optic nerve of the cat: evidence of size groupings and regional organization. J Neurosci 1983; 3:1554-64. [PMID: 6875656].

43. Silveira LC, Russelakis-Carneiro M, Perry VH. The ganglion cell response to optic nerve injury in the cat: differential responses revealed by neurofibrillar staining. J Neurocytol 1994; 23:75-86. [PMID: 8195813].

44. Shou T, Liu J, Wang W, Zhou Y, Zhao K. Differential dendritic shrinkage of alpha and beta retinal ganglion cells in cats with chronic glaucoma. Invest Ophthalmol Vis Sci 2003; 44:3005-10. [PMID: 12824245].

45. Wassle H, Peichl L, Boycott BB. A spatial analysis of on- and off-ganglion cells in the cat retina. Vision Res 1983; 23:1151-60. [PMID: 6649435].

Articles are provided courtesy of Emory University and the Zhongshan Ophthalmic Center, Sun Yat-sen University, P.R. China. The print version of this article was created on 19 November 2021. This reflects all typographical corrections and errata to the article through that date. Details of any changes may be found in the online version of the article.